**RESEARCH ARTICLE**

Particle & Particle Systems Characterization
www.particle-journal.com

# Versatile Approach to Self-Assembly of Surface Modified Nanoparticles into SERS-Active Nanoclusters

*Min Zhang, Jie Liu,* Xun Li, Xiaoyu Zhao, Zhiqun Cheng, and Tian-Song Deng**

**A versatile method is invented to self-assemble gold nanoparticles (GNPs) into nanoclusters (NCs) of various morphologies. By storing the particles in toluene, a highly non-polar solvent, under conditions that ensure particle stability, the success rate of subsequent assembly can be enhanced. Additionally, conducting particle self-assembly at a stirring speed of 200 rpm allows the NCs to maintain a spherical shape. The relative standard deviation (RSD) of Raman spectral peaks of multiple NCs used as surface-enhanced Raman spectroscopy (SERS) substrates is calculated to be less than 10%, effectively addressing the issue of low repeatability when using NCs as SERS substrates. Furthermore, even at an analyte concentration reduced to $10^{-9}$ M, a SERS characteristic peak intensity of approximately $2 \times 10^3$ is measurable, demonstrating the high sensitivity of the assembled structures. Finally, by detecting SERS signals from NCs of varying sizes, the intensities of characteristic peaks tend to converge, eliminating the influence of morphology and size on SERS detection.**

## 1. Introduction

Surface-enhanced Raman scattering (SERS) spectroscopy is a highly valuable surface analytical technique renowned for its non-destructive characteristics and minimal interference in aqueous environments.[1] This technique finds wide-ranging applications in fields such as molecular recognition,[2] practical chemical sensors,[3] and multiplexed antibiotics detection.[4] SERS relies on the optical properties of plasmonic nanoparticles (NPs) that enable efficient electric-field confinement.[5] Consequently, the development of plasmonic NPs has emerged as a key focus in the field of nanotechnology.[6,7] Given the sensitivity of plasmonic NPs to their morphology and surrounding environment,[8,9] numerous strategies have been employed to disperse NPs in polar solvents with precise morphologies and size.[10,11] However, the fabrication of self-assembled nanostructures from functionalized NPs can be enhanced by dispersing them in non-polar solvents following ligand modification.[12,13] By carefully controlling the concentration of hydrophobic ligands and introducing negatively charged spacer molecules, such as disodium cromoglycate (DSCG), it becomes possible to induce the formation of dimers at the water–chloroform interface through electrostatic interaction.[14] In recent years, researchers have leveraged the strong affinity of thiol groups to metal particle surfaces to assemble novel structures.[15,16] Although thiols have an affinity for the surface of NPs, they tend to react with them. On the other hand, the appropriate molecular weight of thiol-terminated polystyrene (PS-SH) can be grafted onto the NPS surface, forming a hydrophobic polystyrene (PS) layer that provides long-term dispersion stability in organic solvents,[17] leading to a significant improvement in the performance of photovoltaic cells.[18,19]

Liz-Marzan et al.[20] demonstrated that different shapes and sizes of NPs can form ordered arrays with pronounced plasmonic coupling at the air-water interface, resulting in highly efficient substrates for SERS. However, apart from gold nanorods (GNRs), the SERS signals measured from other particles are relatively weak and posed challenges for their utilization as substrates for molecular detection. In the field of SERS, various self-assembled structures, such as nanocap arrays,[21] monolayer films,[22,23] self-assembled stripes,[24] and nanoclusters (NCs),[25,26] have been extensively employed as substrates. These nanostructures integrate multiple functionalities into a single system, enabling the formation of multifunctional nanostructures, thus expanding the capabilities of SERS for molecular detection and analysis.[27] NCs are particularly appealing due to their precise control, larger surface area, stronger plasmonic properties and superior thermal stability of constituent particles. These properties not only enhance the amplification of Raman signals from molecules in proximity to plasmonic NCs but also have a nondamaging effect on the sample during SERS testing, allowing for its reuse without compromising its integrity. As a result, these characteristics make NCs highly promising for SERS detection, offering significant potential for advancements in molecular detection and analysis.[28] Additionally, enhancing the range of potential applications, such as SERS and single-particle dark-field scattering,[29–31] as well as the heterogeneity

---

M. Zhang, J. Liu, X. Li, Z. Cheng, T.-S. Deng
School of Electronics and Information Engineering
Hangzhou Dianzi University
Hangzhou 310018, P. R. China
E-mail: liujie4209@hdu.edu.cn; dengts@pku.edu.cn

X. Zhao
College of Materials and Environmental Engineering
Hangzhou Dianzi University
Hangzhou 310018, P. R. China

The ORCID identification number(s) for the author(s) of this article can be found under https://doi.org/10.1002/ppsc.202400034

**DOI: 10.1002/ppsc.202400034**

of NCs, can be achieved through various methods of particle assembly.[32–34] For instance, Miyahara et al.[35] introduced the concept of the spontaneous formation of ordered patterns of NCs on hydrophilic flat substrates using a convective self-assembly method. They were able to manipulate the size of the clusters and maintain a consistently spaced arrangement by controlling the particle concentration and temperature, thereby imparting SERS activity. Another approach involved the combination of electrodeposition and electroless plating to fabricate silver-plated GNPs on indium tin oxide (ITO) glass (Au@Ag_ITO).[36] This hybrid structure exhibited superior SERS performance with a remarkably low detection limit of approximately $10^{-11}$ м for dopamine concentration. An ultrasensitive detection substrate is successfully obtained by assembling suspensions of GNRs with the application of an alternating current (AC) field, which is proposed to enhance the SERS signal.[37] Focused-ion-beam and template-assisted methods were employed to achieve SERS substrates that create nanometer- to micron-sized NCs, involving tens to thousands of NPs. However, these methods have limitation in terms of the range of formed sizes that can be created and may lead to assemblies that are fixed in or on a substrate.[38] As for the Pickering method, it utilizes solvent evaporation to assemble NPs into NCs, and the samples are finally collected in solution, saving costs. Furthermore, this method also retains the highly sensitive SERS signals due to the enhanced electric fields between the particles. For example, a previous study by van Blaaderen et al.[39] demonstrated the self-assembly of silica-coated gold nanorods (GNRs@$SiO_2$) into NCs. This self-assembly process allowed for precise control of the NCs' porosity, interparticle distance, and optical properties, resulting in SERS signals. However, the silica coating on the nanorods effectively reduced the available surface area for probe molecules to interact with the NCs, which weakened their optical properties.

Based on this concept, we propose a method to fabricate self-assembled spherical NCs using ligand binding optimization techniques, applicable to GNPs with various functionalities. Stable NCs were assembled using PS-SH coated GNRs and GNSs under the same conditions, dispersed in water, and utilized as a SERS platform for direct detection of hydrophobic substances, using Nile red as an analyte and clusters as active substrates. The SERS spectra of different particles in the sample showed a small relative standard deviation (RSD), demonstrating the reliability and stability of the SERS technique. The optical resonance of individual NPs reflects information on their structure and interactions with the surrounding environment.

## 2. Results and Discussion

### 2.1. Preparation Building Blocks of GNPs@PS-SH NCs

As a famous and popularly studied nanomaterials, GNPs of surface modification have been widely applied in various fields such as SERS and photothermal conversion,[40,41] owing to its simple synthesis methods and unique optical properties. Here, a straightforward self-assembly process is introduced for synthesizing NCs, which can be applied to GNPs with different morphologies.

Generally, the fabrication of stable NCs typically involves surface modification and self-assembly of NPs. The detailed synthesis process is shown in **Figure 1**. Initially, the preparation of GNRs (GNSs) with good monodispersity was performed, as depicted in Figure S1 (Supporting Information). PS-SH is attached on the surface of GNRs (GNSs) through Au—S bond to increase the stability of GNRs (GNSs). In this process, it is important to mention that post-cleaning, GNRs (GNSs) should be stored briefly in a small amount of aqueous solution to prevent immediate aggregation. Subsequently, a transient state solvent such as THF can be used. Henceforth, surface tension, along with the emulsifier's amphiphilic properties, drives the solution to reduce its surface area and form droplets. Eventually, volatilization of the solution makes the small droplets form stable clusters.

The successful surface modification of NPs is confirmed through various characterization techniques, including UV–vis extinction spectra and optical images. These analyses demonstrated the effective phase transfer of NPs by utilizing PS-SH as both a hydrophobic agent and stabilizer. The full width at half maximum (FWHM) of the spectra is examined to verify the dispersion of GNPs@PS-SH in toluene, and no changes are observed before and after the modification process, indicating the absence of aggregation (**Figure 2**a,b). Additionally, the introduction of PS-SH molecules caused a slight red-shift of the surface plasmon resonance of the GNPs, which is attributed to changes in the refractive index ($n$) of the surrounding medium.[42] The refractive index is related to the optical dielectric constant (ε) of the external medium (solvent, surfactant, support) by the equation:

$$n = \varepsilon^{1/2} \tag{1}$$

In the case of toluene (ε = 2.24) compared to water (ε = 1.77), a higher optical dielectric constant weakens the interaction between free electrons on the particle surface and the incident light field, leading to a red shift in the spectrum.[43] Furthermore, the solubility of GNPs@PS-SH in various solvents (Figure S2, Supporting Information), including toluene, THF, and chloroform, was investigated. Notably, in toluene, the solubility analysis (Figure 2c,d) demonstrated well-separated NPs without any indication of aggregation or changes in color even after an extended period. This observation highlights the exceptional performance of toluene as a solvent, surpassing THF and chloroform in maintaining the integrity of the modified NPs, especially GNRs. The strong affinity of thiol groups for metallic surfaces played a vital role in facilitating the efficient phase transfer of the NPs.

### 2.2. Self-Assembly of GNPs@PS-SH NCs

The fabrication of GNPs@PS-SH into NCs was achieved using the solvent evaporation method, taking inspiration from the method developed by Mason and Bibette.[44] The use of water-in-oil emulsion, instead of oil-in-water emulsion, is suitable for surface-functionalized particles, maintaining the required structural stability and enhancing the biocompatibility of the particles.[45] In our study, the emulsifier, which is composed of dextran and SDS (20:3), functions as a surfactant by forming an interfacial film between the oil and water phases. This film reduces the surface tension of the liquids, thereby preventing delamination or condensation (Figure S3, Supporting Information). The formation of NCs in the emulsion is closely related to

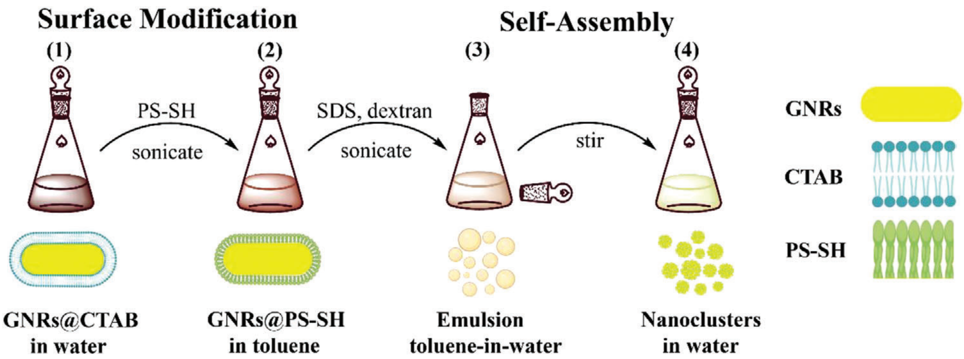

**Figure 1.** Schematic diagram illustrating the formation strategy for GNRs@PS-SH NCs is presented, involving two key steps: surface modification and self-assembly. Four steps described in detail: (1) The as-synthesized GNRs@CTAB were redispersed in water. (2) The phase transfer of GNRs was achieved by transferring them into toluene, resulting in the formation of GNRs@PS-SH. (3) An emulsion was generated by incorporating toluene-in-water phases. (4) The resulting NCs were then dispersed in water for further analysis.

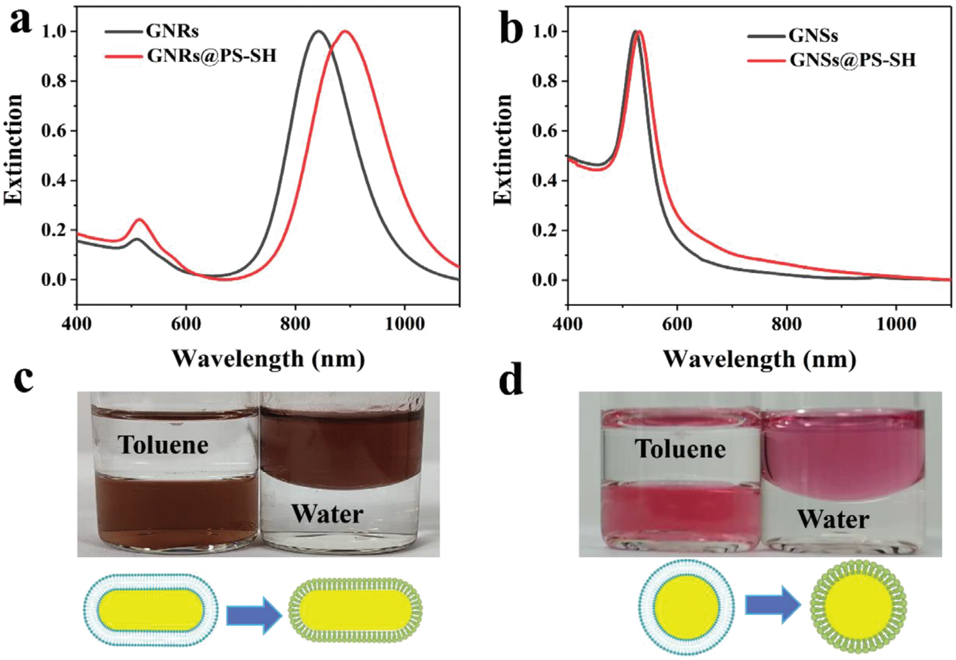

**Figure 2.** Normalized extinction spectra in water (black lines) and in toluene (red lines), for a) GNRs and b) GNSs. Phase transfer of c) GNRs and d) GNSs from water (lower phase) into a solution of PS-SH in toluene (upper phase). The diagrams and glass bottles on left and right depict the same samples before and after phase transfer.

the evaporation rate. At low stirring speeds of 50 rpm, the shear force of the surrounding fluid decreases, causing the particles aggregation and the formation of irregular assemblies (Figure S4a, Supporting Information). Increasing the stirring speed to 200 rpm leads to a gradual approach to equilibrium and relatively unchanged structure (Figure S4b, Supporting Information). However, at high stirring speeds of 500 rpm, the shear force of the particles in the fluid is extremely strong, causing particle dispersion and increased gaps (Figure S4c, Supporting Information).[46]

**Figure 3** illustrates the characterization of NCs formation for two types of particles at a stirring speed of 200 rpm in the emulsion. The SEM images (Figure 3a,c) clearly show the dense arrangement of individual particles, forming uniform-shape NCs. The size distribution of uniform-shape NCs is shown in Figure S5 (Supporting Information), the diameter size of GNRs@PS-SH NCs is 210 ± 72 nm (Figure S5a, Supporting Information) and the diameter size of GNSs@PS-SH NCs is 597 ± 170 nm (Figure S5b, Supporting Information). The relative deviation of the sizes is also within a reasonable range. Figure 3b demonstrates the collective UV–vis extinction spectra of the GNRs@PS-SH NCs solution after the self-assembly process, revealing distinct characteristics indicating side-by-side assembly and noticeable heterogeneity compared to the spectra of GNRs (Figure 2a). Previous studies have reported that side-by-side assembly of GNRs leads to a red-shift of the transverse mode and a blue-shift of the longitudinal mode.[47] In our study, upon self-assembly, the transverse mode of GNRs experienced a significant red-shift of

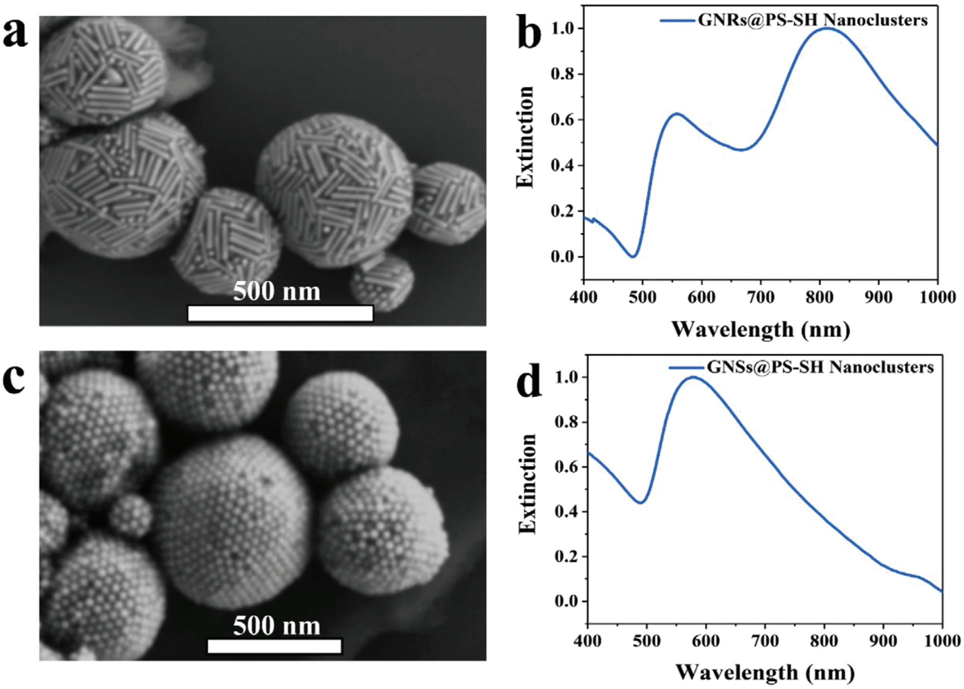

**Figure 3.** Different characterization techniques were employed to analyze the NCs. SEM images of the corresponding a) GNRs@PS-SH NCs and c) GNSs@PS-SH NCs. Normalized extinction spectra of the corresponding NCs dispersed in water for (b,d).

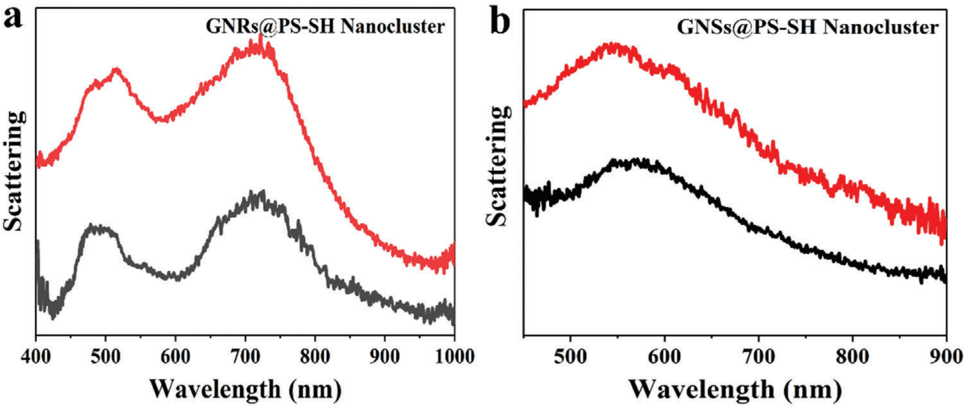

**Figure 4.** Single-particle scattering spectra of a) GNRs@PS-SH NCs and b) GNSs@PS-SH NCs. These spectra are recorded at two distinct spots, represented by the red and black curves, with a dark-field objective with 50× magnification.

43 nm, while the longitudinal mode showed a slight blue-shift of 4 nm accompanied by broader waveforms compared to individual GNRs. Furthermore, the GNSs@PS-SH NCs (Figure 3d) exhibited a red-shift of approximately 70 nm compared to the individual GNSs (Figure 2b). This can be attributed to the pronounced plasmonic coupling, and thus contributing to the observed red-shift and broadening of the spectra.[48]

### 2.3. Single-Particle Dark Field Scattering Spectroscopy of the NCs

Single-particle dark-field spectroscopy has emerged as a powerful tool for investigating the plasmonic properties of individual NPs, including NC, revealing their similar characteristics to NPs in solution. The interaction of particles with the surrounding environment allows for the detection of the optical responses of the particles under various conditions. This technique provides valuable insights into the behavior of individual NPs and their plasmonic properties. **Figure 4a** shows the scattering spectra of GNRs@PS-SH NCs, which exhibit two distinct bands with different intensities. The first band typically falls between 450 and 550 nm, while the second band, which is usually more intense, appears at higher wavelengths within the range of 700 to 750 nm. The stronger bands are likely associated with the longitudinal modes of the rods and the coupling modes between them. This coupling leads to the shift in resonance position, primarily due to changes in the

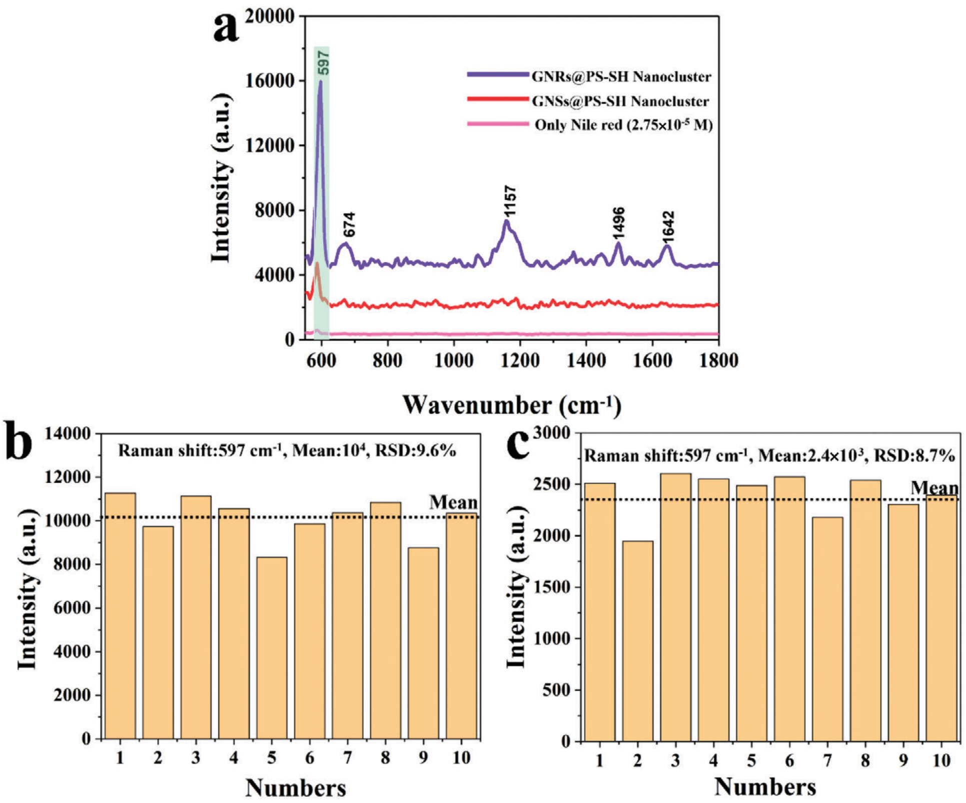

**Figure 5.** a) SERS spectra of Nile red at $2.75 \times 10^{-5}$ M in toluene showed on GNRs@PS-SH NCs and GNSs@PS-SH NCs as substrates for the detection. The reproducibility of Raman intensity of Nile red at 10 different NCs from the same sample. b) GNRs@PS-SH NCs and c) GNSs@PS-SH NCs.

overall aspect ratio of multiple GNRs after coupling, resulting in discrepancies between the dispersion spectrum and the characteristic spectrum of the macroscopic solution.[49] Moreover, the discrepancy could be due to differences in the refractive index of the surrounding environment, while the particles in the solution are surrounded by water ($n = 1.33$), the single particle test is performed under air ($n = 1.0$) conditions. This difference in refractive index could lead to a shift in the resonant position.[50] Similarly, Figure 4b presents the scattering spectra of GNSs@PS-SH NC under identical conditions, exhibiting a blue-shift in spectral peaks. The structured spectra could be attributed to small aggregates consisting of a few single GNP packed closely together or variations in their spacing. These findings underscore the significance of considering the attributes of individual NCs when analyzing their behavior and characteristics. Scattering spectra offer highly sensitive signals, enabling the detection of particles at extremely low concentrations without being affected by background interference. This highlights the robust nature of NCs and their consistent properties across various environmental conditions.

### 2.4. SERS Performances of GNPs@PS-SH NCs

The durability of surface-accessible NCs is essential in applications where direct access to the functional surface necessary. This durability allows the GNCs to maintain their performance even when there are changes in the surface chemistry of their NPs constituents. To ensure a fair comparison of the performances of different GNPs as SERS substrates, standardized methods are employed for phase transferring, self-assembling, and cleaning for all GNPs, regardless of their dimensions and morphology. This standardized approach enables us to accurately evaluate the SERS activity of each GNP and determine their suitability for various sensing applications. To efficiently load the probe analytes onto the GNCs, a coincubation period of 2 h was implemented. This duration ensures sufficient time for the analytes to interact with the GNCs and achieve optimal loading efficiency.

To further demonstrate the effectiveness of the self-assembled NCs as substrates, Nile red is used as a non-polar analyte in a non-polar solvent. The molecular formula of Nile red is shown in Figure S6a (Supporting Information). Detailed experimental procedures can be found in the materials and methods section. **Figure 5a** presents the Raman signal intensity of Nile red molecules on different NCs, with prominent peaks observed at 597 $\text{cm}^{-1}$, along with other low-intensity peaks at 674, 1157, 1496 and 1642 $\text{cm}^{-1}$.[51,52] When using GNPs@PS-SH NCs in SERS measurements, a significant enhancement of vibrational spectra can be achieved, especially GNRs. The main reason for this enhancement is the interaction between light and the free electrons on the metal surface, causing electron oscillation, known as the plasmonic effect, which enhances the electromagnetic field around the metal. The enhanced electromagnetic field interacts with the analyte molecules adsorbed on the metal surface, leading to a substantial enhancement of the Raman signal.[53] In addition, through the FDTD simulations of GNRs and GNSs, obtaining the electric field distributions as shown in Figure S7

(Supporting Information). As illustrated in Figure S7a (Supporting Information), side-by-side aligned GNRs exhibit strong localized electric fields at their ends, while end-to-end aligned GNRs (Figure S7b, Supporting Information) show strong localized electric fields at adjacent locations. In the case of GNSs (Figure S7c, Supporting Information), the electric field intensity between two adjacent spheres is slightly lower. This is consistent with the experimental results, indicating high sensitivity.

The enhancement factor (EF) for the NCs is quantified using the following relation:[39]

$$\mathrm{EF} = \frac{I_\mathrm{S}}{I_\mathrm{R}} \cdot \frac{N_\mathrm{R}}{N_\mathrm{S}} \tag{2}$$

where $I_\mathrm{S}$ and $I_\mathrm{R}$ represent the relative intensity at 597 $\mathrm{cm}^{-1}$ of the NCs@Nile red Raman spectrum and Nile red Raman spectrum, respectively. $N_\mathrm{S}$ and $N_\mathrm{R}$ are the concentration of Nile red absorbed on the substrate for SERS and NR, respectively. With an EF of approximately $10^4$ for the GNRs@PS-SH NCs substrate and approximately $10^3$ for the GNSs@PS-SH NCs substrate, we further delved into investigating the repeatability of NCs as SERS substrates by examining the variation in SERS signal intensity at 597 $\mathrm{cm}^{-1}$. The average intensity of GNRs@PS-SH NC is about $10^4$ (Figure S8a, Supporting Information), with RSD of 9.6% (Figure 5b), and the average intensity of GNs@PS-SH NC is approximately $2.4 \times 10^3$ (Figure S8b, Supporting Information), with RSD of 8.7% (Figure 5c). In addition, it was found that when GNRs@PS-SH and GNSs@PS-SH were subjected to SERS detection, there were differences in the intensity of the characteristic peak of the analyte Nile Red at 597 $\mathrm{cm}^{-1}$ (Figure S9a,b, Supporting Information), with an overall decrease in intensity and inconsistent results. The main reason for this is that after the particles are dropped onto the silicon wafer, solvent evaporation causes the particles to naturally aggregate into clusters, with uneven dispersion of surrounding particles, leading to significant measurement deviations. In contrast, nanoaggregates exhibit stable shapes, higher measurement accuracy, and good reproducibility on the SERS platform. Additionally, we conducted SERS tests on different GNRs@PS-SH NCs and GNSs@PS-SH NCs of the same sample in a dark-field background, as the particle sizes vary in brightness (Figure S10a,b, Supporting Information). Surprisingly, at the same concentration, the characteristic peak intensities of different-sized NCs did not exhibit a significant correlation with their sizes (Figure S11a,b, Supporting Information). This suggests that the size of NCs does not have a pronounced influence on the intensity of its Raman characteristic peaks, possibly due to the non-uniform distribution of analyte droplets on the silicon substrate during the experimental process, which can lead to the formation of coffee rings.[54] Besides that, as the concentration of Nile Red decreases, the signal of the characteristic peak at 597 $\mathrm{cm}^{-1}$ significantly weakens, and the intensity of its characteristic Raman peak can reach $10^3$, indicating a high sensitivity (Figure S12, Supporting Information).

Considering the dispersibility of the self-assembled NCs in water, the polar analyte R6G (molecular formula shown in Figure S6b, Supporting Information) is employed for staining purposes. As shown in Figure S13 (Supporting Information), R6G exhibits three distinct groups of modes. The first group corresponds to the bending of the C—C—C ring within the plane, observed at 613 $\mathrm{cm}^{-1}$. The second group corresponds to the out-of-plane bending of the C—H ring, observed at 769 and 1127 $\mathrm{cm}^{-1}$. The third group exhibits prominent peaks at 1364 and 1512 $\mathrm{cm}^{-1}$, attributed to the ring breathing motion. These vibrations represent the aromatic C—C stretching modes, which can also be observed at lower intensities at 1183, 1312, and 1648 $\mathrm{cm}^{-1}$.[55] GNRs exhibit a stronger electric field compared to GNSs due to their shape's stronger polarization effect. This is attributed to the larger aspect ratio of GNRs, which results in a highly localized concentration effect at the two tips of the rod, thereby enhancing the intensity of the electric field.[56]

## 3. Conclusion

In conclusion, we have developed a universal approach for the self-assembly of plasmonic NPs into NCs through surface modification. Comparison of modified GNPs in different solvents revealed that toluene, a highly non-polar solvent, effectively maintains particle stability for ideal self-assembly conditions. Lower speeds (200 rpm) during solvent evaporation were found to preserve spherical shape, offering a practical method for shape control. Consistency in dark-field scattering spectra of individual NCs compared to extinction spectra in aqueous solutions is observed at both macroscopic and microscopic levels. The low RSD (<10%) in analyte molecule intensities at characteristic peak positions for different NCs indicates good repeatability during usage, essential for enhancing SERS detection accuracy and reliability. Even at a reduced analyte concentration of $10^{-9}$ M, NCs exhibited high SERS activity with a Raman intensity of $2 \times 10^3$. Furthermore, the study on NCs size's influence on SERS signals showed consistent Raman spectral intensities across different cluster sizes, eliminating the size impact on SERS signals. This underscores the plasmonic properties and stability of self-assembled NCs, highlighting their potential for practical applications.

## 4. Experimental Section

*Materials*: All chemicals were obtained from commercial suppliers and used without further purification. Hexadecyltrimethylammonium bromide (CTAB, >99.0%) was purchased from TCI America. Chloroauric acid ($\mathrm{HAuCl_4}$), L-ascorbic acid (AA, >99.99%), rhodamine 6G (R6G, 95%), hydrochloric acid (HCl, 37 wt% in water), cetyltrimethylammonium chloride (CTAC, 99%), sodium dodecyl sulfate (SDS, 92.5%–100.5%), dextran, Nile red, methanol (99.5%), and cyclohexane (99.5%) were purchased from Shanghai Macklin Biochemical Technology Co., Ltd. Silver nitrate ($\mathrm{AgNO_3}$, >99.8%), sodium oleate (NaOL, >99.88%), sodium borohydride ($\mathrm{NaBH_4}$, >98%), and tetrahydrofuran (THF, 99.0%) were purchased from Shanghai Aladdin Biochemical Technology Co., Ltd. Thiol-terminated polystyrene (PS-SH, average $M_n = 11000$, PDI $\leq 1.1$) was purchased form MKCH2403. Toluene (TOL, ≥99.5%) was purchased from National Pharmaceutical Group Chemical Reagent Co., Ltd. Ultrapure water (>18.2 MΩ) obtained from a Milli-Q water system was used in all experiments. All glassware were cleaned using freshly prepared aqua regia (HCl: $\mathrm{HNO_3}$ in a 3:1 ratio by volume) followed by rinsing with copious amounts of water.

*Synthesis of NPs: Growth of the GNRs*: Monodisperse GNRs (87.5 ± 5.6 nm in length; 21.2 ± 2.3 nm in width) were synthesized using a seed-mediated growth method.[57] First, 0.25 mL of $\mathrm{HAuCl_4}$ ($10 \times 10^{-3}$ M) solution was mixed with 10 mL of CTAB (0.1 M) solution, followed by the addition of 600 µL of freshly prepared ice-cold $\mathrm{NaBH_4}$ ($10 \times 10^{-3}$ M) solution under vigorous stirring (1200 rpm) for 2 min. The mixture was allowed to incubate for at least 30 min before use. The growth solution was prepared by dissolving 192 mL of CTAB (0.1 M) and 81 mL of NaOL ($50 \times 10^{-3}$ M) in a 500 mL flask. Then, 18 mL of $AgNO_3$ ($4 \times 10^{-3}$ M) solution was added. The solution was left undisturbed for 15 min at 30 °C, followed by the addition of 25 mL of $HAuCl_4$ ($10 \times 10^{-3}$ M) solution and 164.75 mL of water. The resulting colorless solution was then stirred at 400 rpm for 15 min upon the addition of 18 mL of HCl (1.0 M) solution. Finally, 1.25 mL of AA ($64 \times 10^{-6}$ M) and 400 µL of gold seed solution were added under vigorous stirring (1200 rpm) for 30 s. The mixture was left undisturbed for 12 h. The solution was centrifuged at 7000 rpm for 15 min, repeated twice, to obtain the final products. The pellet was then concentrated in 125 mL of CTAB ($1.6 \times 10^{-3}$ M) solution to remove excess reactants.

*Growth of the GNSs*: The GNSs (21.7 ± 2.0 nm in diameter) were synthesized using a seed-mediated growth method.[58] First, 0.25 mL of $HAuCl_4$ ($10 \times 10^{-3}$ M) solution was mixed with 9.75 mL of CTAB (0.1 M) solution. This mixture was then rapidly added to 600 µL of freshly prepared ice-cold $NaBH_4$ ($10 \times 10^{-3}$ M) solution under vigorous stirring. The resulting mixture solution was kept under slow stirring (160 rpm) for 3 h at room temperature. Next, 120 µL of the as-prepared seed solution was added to a growth solution composed of 9.75 mL of CTAB (0.1 M) solution, 190 mL of water, 4 mL of $HAuCl_4$ ($10 \times 10^{-3}$ M) solution, and 15 mL of AA (0.1 M). The solution was gently shaken and then left undisturbed for 12 h at room temperature. The resultant solution was centrifuged at 14 000 rpm for 30 min, repeated twice, to obtain the final products. The pellet was then concentrated four times into 55.0 mL of CTAB ($20 \times 10^{-3}$ M) solution.

*Surface Modification of NPs*: PS-SH-based ligands were attached to the NPs surface by a simple method with some change.[17,59] First, as-synthesized GNPs (4 mL) were concentrated into 100 µL aqueous solution was injected into the solution of PS-SH in THF (0.4 mg mL$^{-1}$, 2 mL). Then, the mixture solution was sonicated for 2 h and undisturbed overnight at room temperature. The solution was purified by methanol at 7000 or 12 000 rpm for 30 min and toluene at 7000 or 12 000 rpm for 30 min. The samples were finally concentrated into 2 mL toluene.

*Self-Assembly of NPs*: The self-assembly of NCs was achieved using an oil-in-water emulsion method.[44] First, the as-synthesized GNRs@PS-SH or GNSs@PS-SH were dispersed in 200 µL of toluene and added to a mixture containing 160 mg of dextran and 24 mg of SDS in 4 mL of water. The solution was subjected to sonication for 2 min (power at 40.0 kHz; electric current at 1.1 A) and then gently stirred at 50, 200, and 500 rpm for 12 h at room temperature, respectively. The resulting products were collected by centrifugation at 2000 rpm for 5 min, repeated twice, and then redispersed in an aqueous solution.

*SERS Using GNPs@PS-SH NCs and GNPs@PS-SH*: SERS measurements[39] were conducted using a BX53M microscope equipped with a NOVA 2S-EX (325–1100 nm) Raman spectrometer. The samples were excited with a 785 nm laser source at a power of 200 mW. For the SERS measurements, 20 µL of sample (GNPs@PS-SH NCs or GNPs@PS-SH) were drop-casted onto dry silicon wafers. Prior to the deposition of sample, the wafers were cleaned by sonication in water with acetone for 5 min, followed by two rinses with ethanol. The surface of the sample was loaded with a Nile red solution at different concentrations of $2.75 \times 10^{-5}$ M or $2.75 \times 10^{-9}$ M in toluene, and a R6G solution with a concentration of $10^{-5}$ M in water. The wafer was then dried and placed under the BX53M microscope. A 50x air objective was used with a laser spot size of approximately 1 µm. Typically, a laser power of 70% (≈140 mW), an exposure time of 1 s, and 5 accumulations were utilized during the SERS measurements.

*Single-Particle Dark-Field Scattering Measurements*: Single-particle dark-field scattering measurements[60] were conducted using an Olympus BX53 optical microscope equipped with a halogen lamp (100 W) and a NOVA 2S-EX spectrometer. A dark-field objective with a numerical aperture of 0.80 and a magnification of 100× was employed to both excite the NCs with white light and collect the scattered light. The scattered light was directed toward the entrance slit of the monochromator. Subsequently, the scattered spectra from individual NCs were acquired by subtracting the background spectra obtained from adjacent regions without particles. To normalize the data, the acquired spectra were divided by the pre-calibrated response curve of the entire optical system.

*Finite-Difference-Time-Domain (FDTD) Simulations*: The electric field simulations of GNPs were calculated using FDTD method, which is an explicit time-marching algorithm used to solve Maxwell's curl equations on a discretized spatial grid. The FDTD simulations were carried out with a software package from FDTD Solutions (Lumerical Solutions, Inc.). A light pulse in the wavelength range of 300–1100 nm was launched into a box containing GNPs to simulate a propagating plane light wave interacting with the GNPs. The GNPs were surrounded by a virtual boundary with an appropriate size. The GNPs and its surrounding medium inside the boundary were divided into meshes size of 1 nm. The sizes of the GNPs were taken from their average values. The gap between particles set at 4 nm. The refractive index of the surrounding medium was set to be 1.33 (water).

*Characterizations*: All absorption measurements were captured on a UV-1900i spectrophotometer (SHIMADZU, Japan) with a 10.0 mm optical path, whereby a glass cuvette filled with Milli-Q water or toluene was used as the reference. Transmission electron microscopy (TEM) images were captured on a HT-7700 microscope (HITACHI, Japan) operating at 100.0 kV. Scanning electron microscopy (SEM) images were captured using Gemini SEM 300 (Zeiss, Germany), both of which were operated at 3.0 kV. SERS experiments were recorded on a NOVA 2S-EX (325-1100 nm) Raman spectrometer under a 785 nm laser source excitation with 200 mW x 70% laser power (Ideal Optics, Shanghai, China). Optical microscopy images were captured on a BX53M microscope (Olympus, Japan).

## Supporting Information

Supporting Information is available from the Wiley Online Library or from the author.

## Acknowledgements

The authors thank Sudan Shen for her assistance in TEM at State Key Laboratory of Chemical Engineering (Zhejiang University). The authors acknowledge financial support from Zhejiang Provincial Natural Science Foundation (Grant: LY24F050008), Zhejiang Provincial Educational Ministry Scientific Research Project (Grant: Y202352284), and National Natural Science Foundation of China (NSFC, Grant: 61905056). This work was also supported by National Key Research and Development Program of China (Grant: 2018YFE0207500), the National Natural Science Foundation (Grant: 91938201 and 61871169), Zhejiang Provincial Natural Science Foundation (Grant: LZ20F010004) and Project of Ministry of Science and Technology (Grant: D20011).

## Conflict of Interest

The authors declare no conflict of interest.

## Data Availability Statement

The data that support the findings of this study are available in the Supporting Information of this article.

## Keywords

gold nanoparticles, gold nanorods, nanoclusters, self-assembly, surface-enhanced Raman scattering

Received: February 22, 2024
Revised: March 20, 2024

[1] N. Yang, T. T. You, Y. K. Gao, C. M. Zhang, P. G. Yin, *J. Agric. Food Chem.* **2018**, *66*, 6889.
[2] E. Papadopoulou, S. E. Bell, *Angew. Chem., Int. Ed.* **2011**, *50*, 9058.
[3] C. Ma, M. J. Trujillo, J. P. Camden, *ACS Appl. Mater. Interfaces* **2016**, *8*, 23978.
[4] X. Peng, D. Li, Y. Li, H. Xing, W. Deng, *J. Mater. Chem. B* **2021**, *9*, 1123.
[5] N. J. Halas, S. Lal, W. S. Chang, S. Link, P. Nordlander, *Chem. Rev.* **2011**, *111*, 3913.
[6] S. Haque, S. Tripathy, C. R. Patra, *Nanoscale* **2021**, *13*, 16405.
[7] Y. Ma, X. Liu, X. Wei, J. Le, Y. Fu, Q. Han, H. Ji, Z. Yang, H. Wu, *Langmuir* **2021**, *37*, 4578.
[8] J. Gong, G. Li, Z. Tang, *Nano Today* **2012**, *7*, 564.
[9] M. Grzelczak, J. Perez-Juste, P. Mulvaney, L. M. Liz-Marzan, *Chem. Soc. Rev.* **2008**, *37*, 1783.
[10] A. Guerrero-Martínez, S. Barbosa, I. Pastoriza-Santos, L. M. Liz-Marzán, *Curr. Opin. Colloid Interface Sci.* **2011**, *16*, 118.
[11] N. Li, P. Zhao, D. Astruc, *Angew. Chem., Int. Ed.* **2014**, *53*, 1756.
[12] J. Zhou, H. Liu, T. Wang, Y. Li, J. Zhang, Z. Lu, Y. Fu, F. Li, *Chem. Commun.* **2014**, *50*, 14547.
[13] M. Zhang, T. S. Deng, Z. Cheng, *ChemistrySelect* **2023**, *8*, 202301065.
[14] S. Yang, X. Ni, X. Yin, B. Kante, P. Zhang, J. Zhu, Y. Wang, X. Zhang, *Nat. Nanotechnol.* **2014**, *9*, 1002.
[15] Y. Lee, J. Jang, J. Yoon, J. W. Choi, I. Choi, T. Kang, *Chem. Commun.* **2019**, *55*, 3195.
[16] M. Lista, D. Z. Liu, P. Mulvaney, *Langmuir* **2014**, *30*, 1932.
[17] X. Yue, X. Liu, N. Yan, W. Jiang, *J. Phys. Chem. C* **2020**, *124*, 20458.
[18] J. S. Metzman, A. U. Khan, B. A. Magill, G. A. Khodaparast, J. R. Heflin, G. Liu, *ACS Appl. Energy Mater.* **2019**, *2*, 2475.
[19] Y. J. Woo, K. H. Park, O. O. Park, D. H. Wang, *Org. Electron.* **2015**, *16*, 118.
[20] A. B. Serrano-Montes, D. Jimenez de Aberasturi, J. Langer, J. J. Giner-Casares, L. Scarabelli, A. Herrero, L. M. Liz-Marzan, *Langmuir* **2015**, *31*, 9205.
[21] Y. Wang, X. Zhao, L. Chen, S. Chen, M. Wei, M. Gao, Y. Zhao, C. Wang, X. Qu, Y. Zhang, J. Yang, *Langmuir* **2014**, *30*, 15285.
[22] L. Song, Y. Huang, Z. Nie, T. Chen, *Nanoscale* **2020**, *12*, 7433.
[23] L. Wang, Y. Zhang, Y. Yang, J. Zhang, *Materials* **2018**, *11*, 1199.
[24] I. Ahmad, F. Derkink, T. Boulogne, P. Bampoulis, H. J. W. Zandvliet, H. U. Khan, R. Jan, E. S. Kooij, *Beilstein J. Nanotechnol.* **2019**, *10*, 696.
[25] X. Yuan, M. I. Setyawati, A. S. Tan, C. N. Ong, D. T. Leong, J. Xie, *NPG Asia Mater.* **2013**, *5*, e39.
[26] S. Zhao, H. Zhang, S. D. House, R. Jin, J. C. Yang, R. Jin, *ChemElectroChem* **2016**, *3*, 1225.
[27] J. Kumar, R. Thomas, R. S. Swathi, K. G. Thomas, *Nanoscale* **2014**, *6*, 10454.
[28] Y. Zhang, Z. Ye, C. Li, Q. Chen, W. Aljuhani, Y. Huang, X. Xu, C. Wu, S. E. J. Bell, Y. Xu, *Nat. Commun.* **2023**, *14*, 1392.
[29] M. Hu, C. Novo, A. Funston, H. Wang, H. Staleva, S. Zou, P. Mulvaney, Y. Xia, G. V. Hartland, *J. Mater. Chem.* **2008**, *18*, 1949.
[30] X. Tian, Y. Zhou, S. Thota, S. Zou, J. Zhao, *J. Phys. Chem. C* **2014**, *118*, 13801.
[31] H. Z. Zhang, R. S. Li, P. F. Gao, N. Wang, G. Lei, C. Z. Huang, J. Wang, *Nanoscale* **2017**, *9*, 3568.
[32] S. L. Kleinman, R. R. Frontiera, A. I. Henry, J. A. Dieringer, R. P. Van Duyne, *Phys. Chem. Chem. Phys.* **2013**, *15*, 21.
[33] M. Wang, N. Jing, I. H. Chou, G. L. Cote, J. Kameoka, *Lab Chip* **2007**, *7*, 630.
[34] C. Zhang, Z. Li, S. Qiu, W. Lu, M. Shao, C. Ji, G. Wang, X. Zhao, J. Yu, Z. Li, *Nanophotonics* **2021**, *11*, 33.
[35] S. Watanabe, Y. Mino, Y. Ichikawa, M. T. Miyahara, *Langmuir* **2012**, *28*, 12982.
[36] V. D. Phung, W. S. Jung, T. A. Nguyen, J. H. Kim, S. W. Lee, *Nanoscale* **2018**, *10*, 22493.
[37] J. Dong, J. Yuan, Y. Cao, Y. Zhao, Q. Han, W. Gao, T. Li, L. Zhu, J. Qi, *Opt. Lett.* **2022**, *47*, 6365.
[38] C. Hanske, G. González-Rubio, C. Hamon, P. Formentín, E. Modin, A. Chuvilin, A. Guerrero-Martínez, L. F. Marsal, L. M. Liz-Marzán, *J. Phys. Chem. C* **2017**, *121*, 10899.
[39] J. E. S. van der Hoeven, H. Gurunarayanan, M. Bransen, D. A. M. de Winter, P. E. de Jongh, A. van Blaaderen, *Adv. Funct. Mater.* **2022**, *32*, 2200148.
[40] C. Li, S. Li, A. Qu, H. Kuang, L. Xu, C. Xu, *Adv. Funct. Mater.* **2020**, *30*, 2001451.
[41] L. Song, N. Qiu, Y. Huang, Q. Cheng, Y. Yang, H. Lin, F. Su, T. Chen, *Adv. Opt. Mater.* **2020**, *8*, 1902082.
[42] M. Chanana, L. M. Liz-Marzán, *Nanophotonics* **2012**, *1*, 199.
[43] Z. V. Saponjic, R. Csencsits, T. Rajh, N. M. Dimitrijevic, *Chem. Mater.* **2003**, *15*, 4521.
[44] T. G. Mason, J. Bibette, *Langmuir* **1997**, *13*, 4600.
[45] Y. P. Jia, K. Shi, J. F. Liao, J. R. Peng, Y. Hao, Y. Qu, L. J. Chen, L. Liu, X. Yuan, Z. Y. Qian, X. W. Wei, *Small Methods* **2020**, *4*, 1900799.
[46] M. Eftekhari, K. Schwarzenberger, S. Heitkam, A. Javadi, A. Bashkatov, S. Ata, K. Eckert, *Langmuir* **2021**, *37*, 13244.
[47] N. Khlebtsov, L. Dykman, *Chem. Soc. Rev.* **2011**, *40*, 1647.
[48] D. Zámbó, A. Deák, *Period. Polytech., Chem. Eng.* **2016**, *60*, 244.
[49] C. Julien-Rabant, A. Débarre, R. Métivier, G. Laurent, *J. Opt.* **2015**, *17*, 114018.
[50] B. N. Khlebtsov, V. A. Khanadeyev, N. G. Khlebtsov, *Opt. Spectrosc.* **2011**, *104*, 282.
[51] J. A. Kraai, A. X. Wang, G. L. Rorrer, *Adv. Mater. Interfaces* **2020**, *7*, 2000191.
[52] A. N. Ramya, P. S. Ambily, B. S. Sujitha, M. Arumugam, K. K. Maiti, *Algal Res.* **2017**, *25*, 200.
[53] A. D. McFarland, M. A. Young, J. A. Dieringer, R. P. V. Duyne, *J. Phys. Chem. B* **2005**, *109*, 11279.
[54] X. Li, X. Chen, J. Liu, X. Zhao, J. Liu, Z. Cheng, T. S. Deng, *Nanoscale* **2023**, *15*, 12270.
[55] F. Tian, F. Bonnier, A. Casey, A. E. Shanahan, H. J. Byrne, *Anal. Methods* **2014**, *6*, 9116.
[56] E. Petryayeva, U. J. Krull, *Anal. Chim. Acta* **2011**, *706*, 8.
[57] X. C. Ye, C. Zheng, J. Chen, Y. Gao, C. B. Murray, *Nano Lett.* **2013**, *13*, 765.
[58] Q. Ruan, L. Shao, Y. Shu, J. Wang, H. Wu, *Adv. Opt. Mater.* **2014**, *2*, 65.
[59] Y. Chen, J. Fu, K. C. Ng, Y. Tang, W. Cheng, *Cryst. Growth Des.* **2011**, *11*, 4742.
[60] N. Jiang, L. Shao, J. Wang, *Adv. Mater.* **2014**, *26*, 3282.

Particle
& Particle Systems Characterization

# Supporting Information

for *Part. Part. Syst. Charact.*, DOI 10.1002/ppsc.202400034

# Versatile Approach to Self-Assembly of Surface Modified Nanoparticles into SERS-Active Nanoclusters

*Min Zhang, Jie Liu*, Xun Li, Xiaoyu Zhao, Zhiqun Cheng and Tian-Song Deng**

# Supporting Information

# Versatile Approach to Self-Assembly of Surface Modified Nanoparticles into SERS-Active Nanoclusters

*Min Zhang*[†], *Jie Liu*[†, *], *Xun Li*[†], *Xiaoyu Zhao*[‡], *Zhiqun Cheng*[†], *Tian-Song Deng*[†, *]

[*] *Corresponding author. E-mail: dengts@pku.edu.cn; liujie4209@hdu.edu.cn*

[†] School of Electronics and Information Engineering, Hangzhou Dianzi University, Hangzhou 310018, P. R. China.

[‡] College of Materials and Environmental Engineering, Hangzhou Dianzi University, Hangzhou 310018, P. R. China.

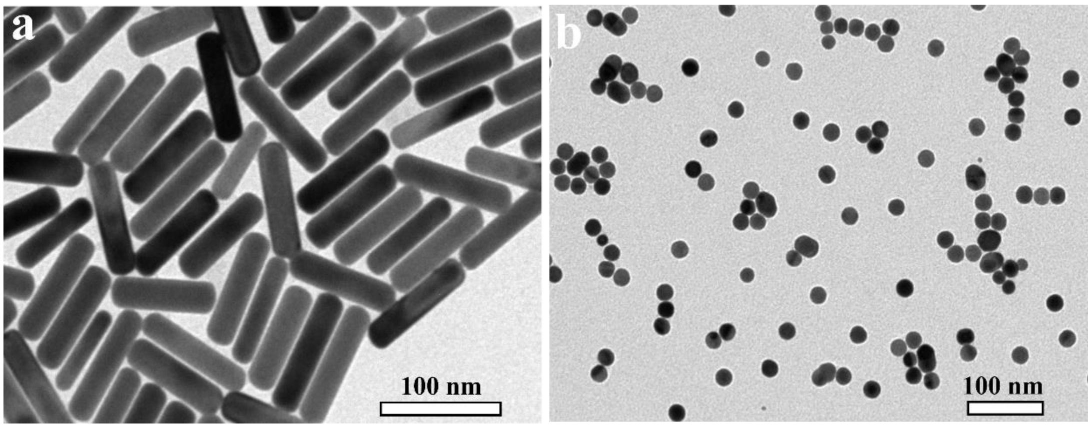

**Figure S1.** (a) TEM images of GNRs with 87.5 ± 5.6 nm in length and 21.2 ± 2.3 nm in width, and (b) GNSs with 21.7 ± 2.0 nm in diameter.

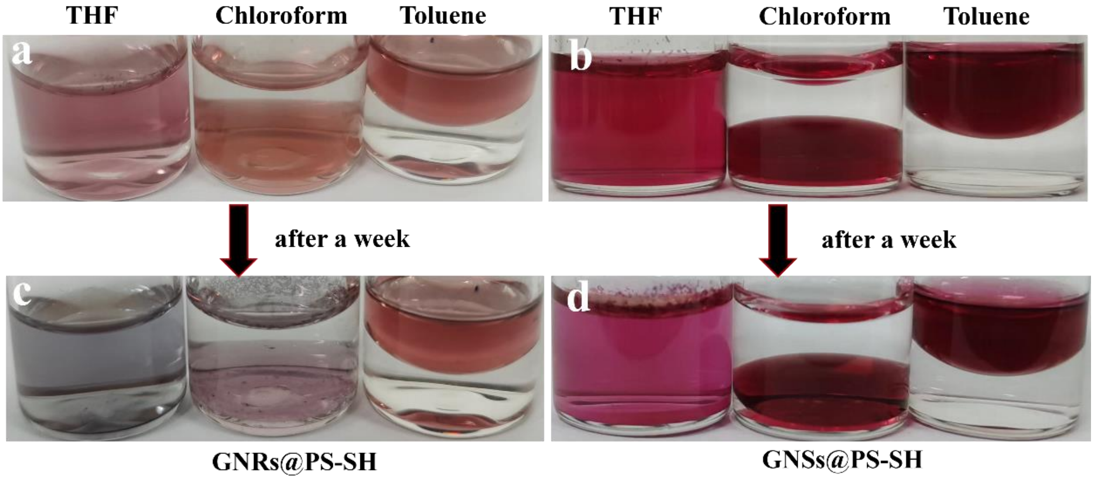

**Figure S2.** (a) GNRs@PS-SH and (b) GNSs@PS-SH were dispersed in THF, chloroform and toluene at a volume ratio of water / solvent =1:1, and (c, d) after a week for solution.

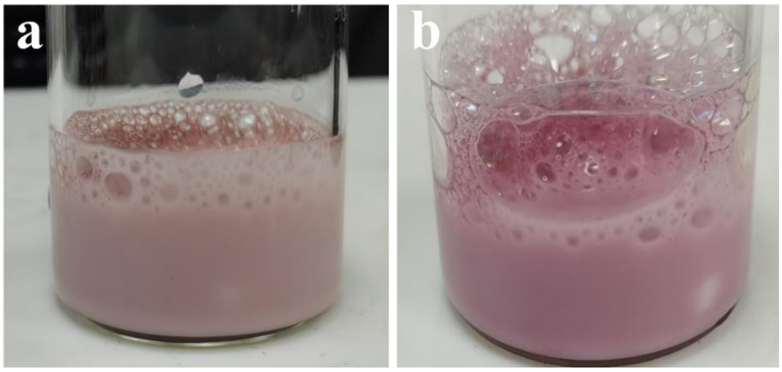

**Figure S3.** Oil-in-water emulsions of (a) GNRs@PS-SH, and (b) GNSs@PS-SH.

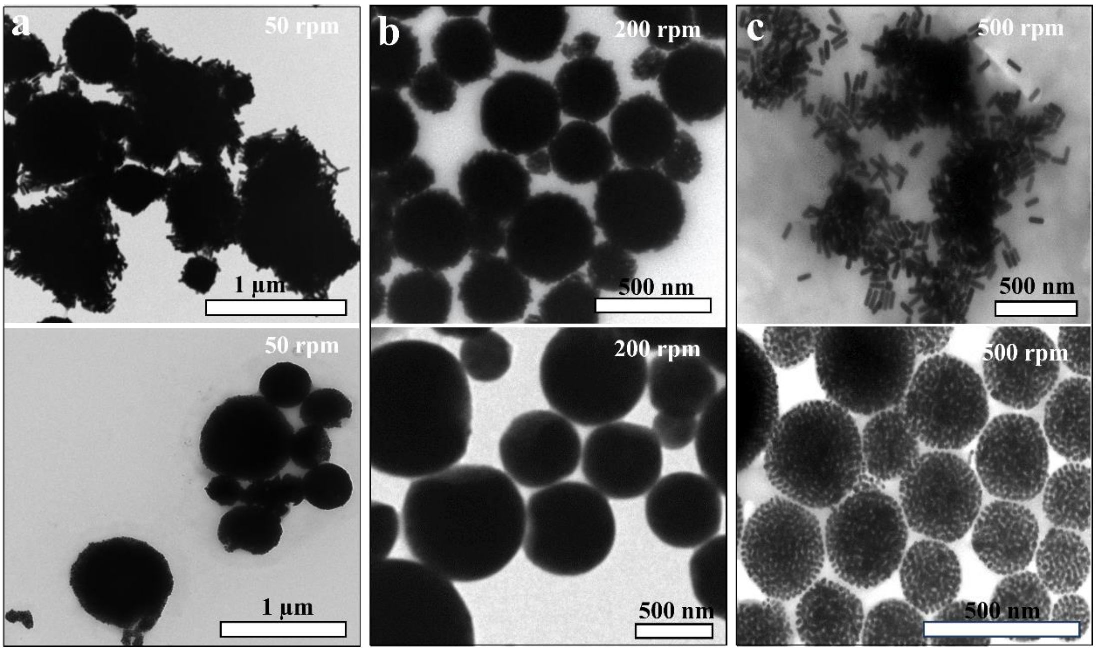

**Figure S4**. (a-c) TEM images of the formed NCs during the evaporation of emulsion of GNRs@PS-SH (upper row) and GNSs@PS-SH (lower row) at different stirring speeds with 50 rpm, 200 rpm and 500 rpm, respectively.

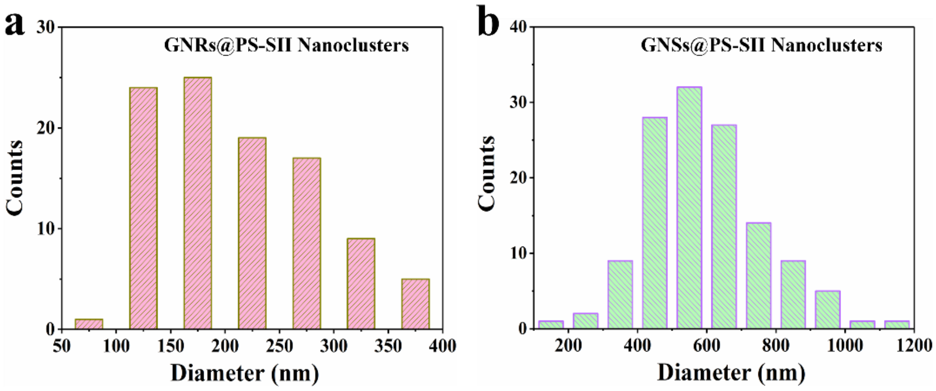

**Figure S5.** (a) Histogram shows GNRs@PS-SH NCs with 210 ± 72 nm in diameters , (b) GNSs@PS-SH NCs with 597 ± 170 nm in diameters.

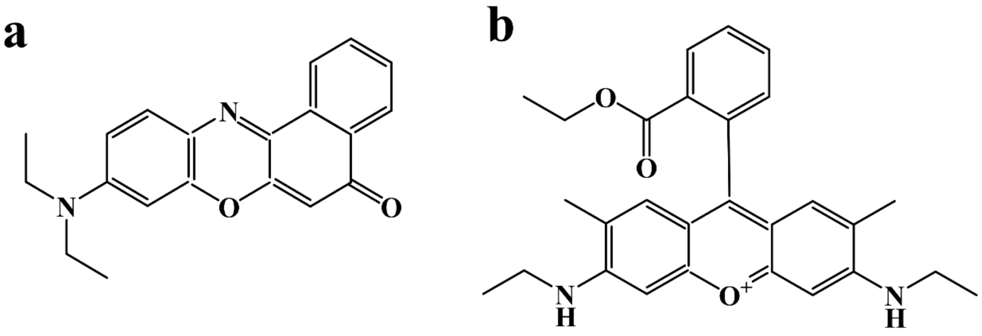

**Figure S6.** Analyte molecular structures of Nile red (a) and R6G (b).

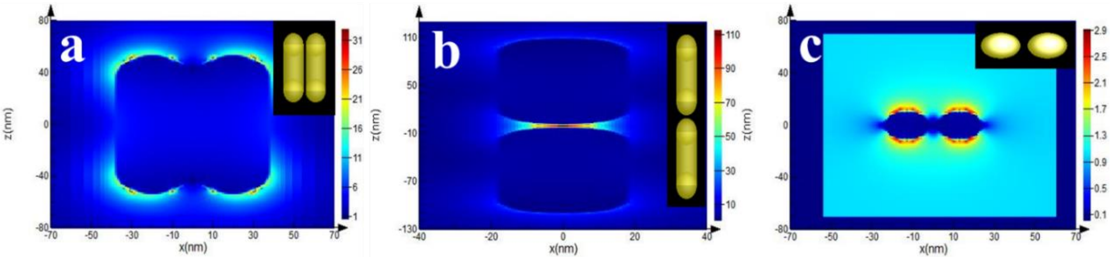

**Figure S7**. Electric field distributions obtained by FDTD simulations illustrate that the plasmonic coupling effect between the GNPs. (a) Two GNRs of the same size as the model in arranged side-by-side, (b) two GNRs of the same size as the model in arranged head-to-head, and (c) two GNSs of the same size as the model.

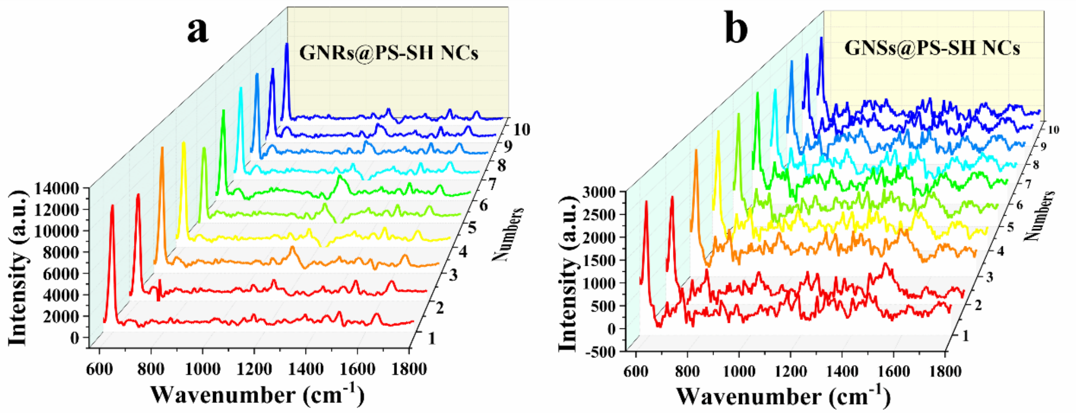

**Figure S8**. SERS spectra of Nile red at 2.75 ×$10^{-5}$ M in toluene showed on 10 different (a) GNRs@PS-SH NCs and (b) GNSs@PS-SH NCs, from the same sample, respectively. The Raman measurements were recorded with a 785 nm laser, 200 mW × 70% laser power.

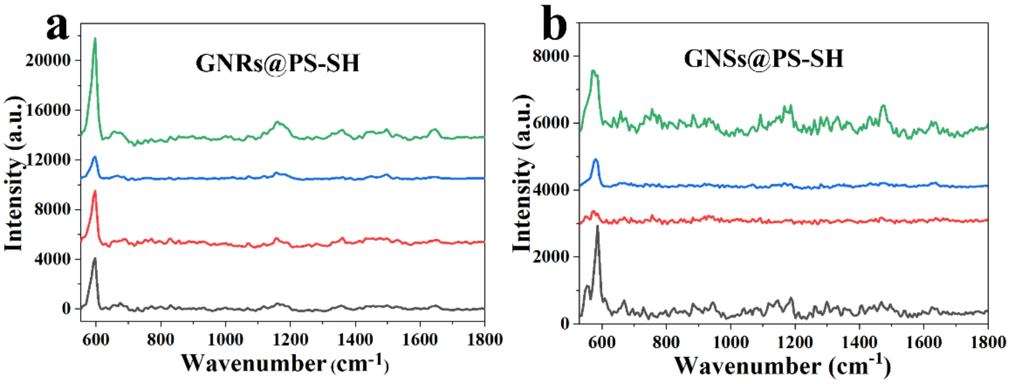

**Figure S9.** SERS spectra of Nile red at 2.75×$10^{-5}$ M in toluene showed on (a) GNRs@PS-SH and (b) GNSs@PS-SH. The Raman measurements were recorded with a 785 nm laser, 200 mW×70% laser power.

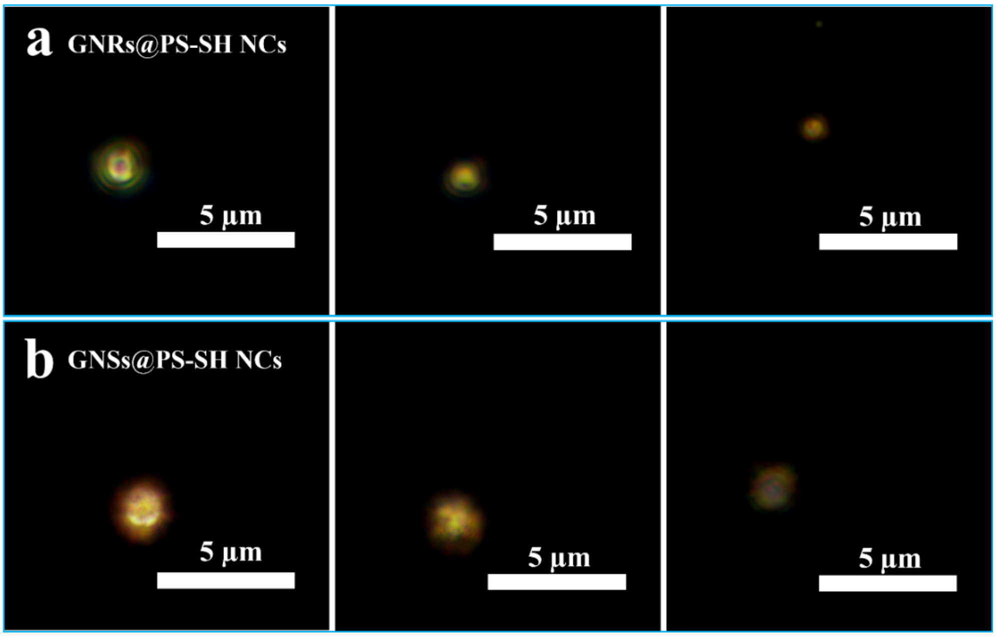

**Figure S10.** Photos of different nanoclusters under the background of dark field. (a) GNRs@PS-SH NCs, (b) GNSs@PS-SH NCs.

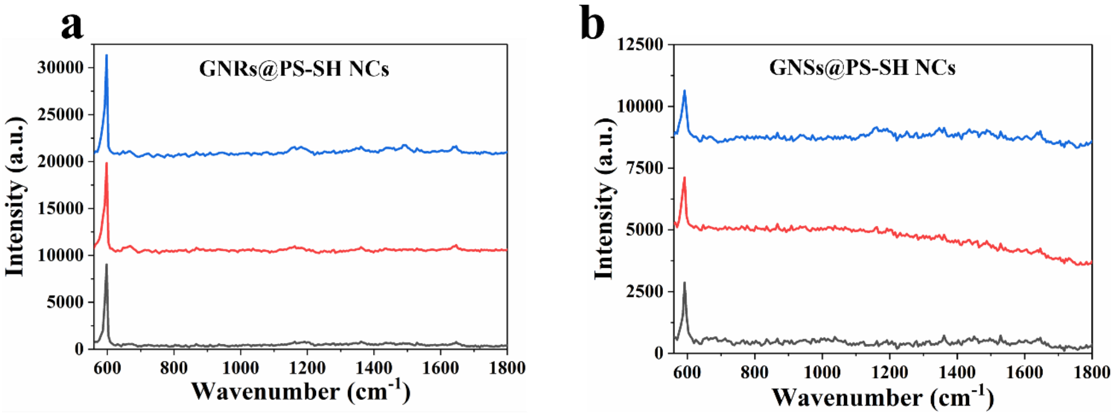

**Figure S11**. SERS performance of different sizes of the (a) GNRs@PS-SH NCs and (b) GNSs@PS-SH NCs. The concentration of Nile red is $2.75\times10^{-5}$ M.

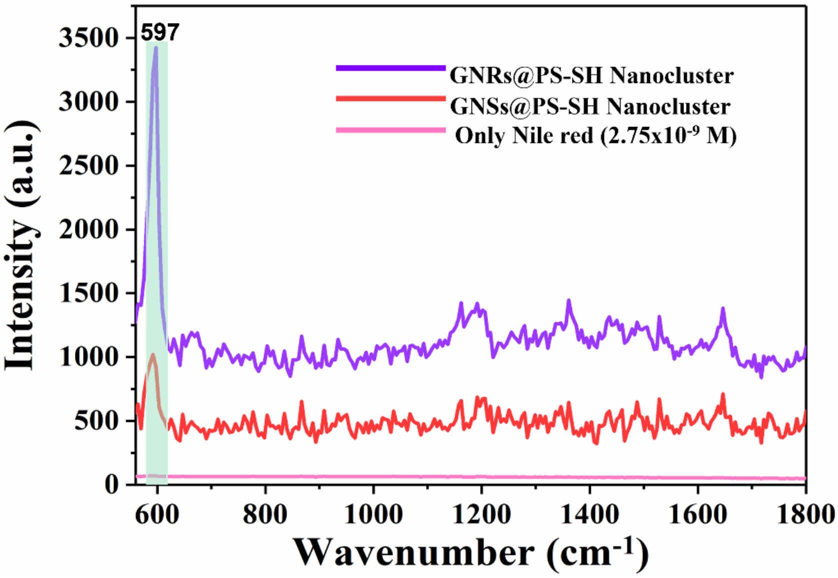

**Figure S12**. SERS spectra of Nile red at $2.75\times10^{-9}$ M in toluene showed on GNRs@PS-SH NCs and GNSs@PS-SH NCs as substrates for the detection.

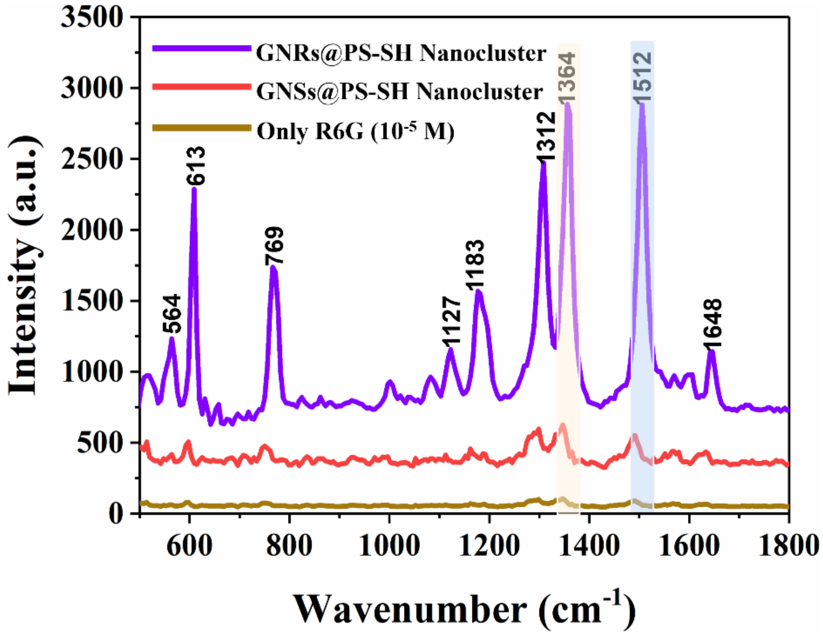

**Figure S13.** SERS spectra of R6G at $10^{-5}$ M in water showed on GNRs@PS-SH NCs and GNSs@PS-SH NCs as substrates for the detection.